PCCP

# Identification of the Acetaldehyde Oxide Criegee Intermediate Reaction Network in the Ozone-Assisted Low-Temperature Oxidation of trans-2-Butene



| | |
|---|---|
| Journal: | *Physical Chemistry Chemical Physics* |
| Manuscript ID | CP-ART-07-2021-003126.R1 |
| Article Type: | Paper |
| Date Submitted by the Author: | 16-Sep-2021 |
| Complete List of Authors: | Conrad, Alan; University of Central Florida<br>Hansen, Nils; Sandia National Laboratories, Combustion Research Facility<br>Jasper, Ahren; Argonne National Laboratory<br>Thomason, Natasha; University of Central Florida<br>Hidalgo-Rodriguez, Laura; University of Central Florida<br>Treshock, Sean ; University of Central Florida<br>Popolan-Vaida, Denisia; University of Central Florida, Department of Chemistry |
| | |

# Identification of the Acetaldehyde Oxide Criegee Intermediate Reaction Network in the Ozone-Assisted Low-Temperature Oxidation of *trans*-2-Butene

Alan R. Conrad,[a] Nils Hansen,[b] Ahren W. Jasper,[c] Natasha K. Thomason,[a] Laura Hidaldo-Rodrigues,[a] Sean P. Treshock,[a] and Denisia M. Popolan-Vaida[a,*]

[a] *Department of Chemistry, University of Central Florida, Orlando, FL 32816, USA*
[b] *Combustion Research Facility, Sandia National Laboratories, Livermore, CA 94551, USA*
[c] *Chemical Sciences and Engineering Division, Argonne National Laboratory, Lemont, IL 60439, USA*

## Abstract

Uni- and bi-molecular reactions involving Criegee intermediates (CIs) have been the focus of many studies due to the role these molecules play in atmospheric chemistry. The reactivity of CIs is known to strongly depend on their structure. The reaction network of the second simplest CI, acetaldehyde oxide ($CH_3CHOO$), is investigated in this work in an atmospheric pressure jet-stirred reactor (JSR) during the ozonolysis of *trans*-2-butene to explore the kinetic pathways relevant to atmospheric chemistry and low-temperature combustion. The mole fraction profiles of reactants, intermediates, and final products are determined by means of molecular-beam mass spectrometry in conjunction with single-photon ionization employing tunable synchrotron-generated vacuum ultraviolet radiation. A network of CI reactions is identified in the temperature region below 600 K, characterized by CIs addition to *trans*-2-butene, water, formaldehyde, formic acid, and methanol. No sequential additions of the $CH_3CHOO$ CI are observed, in contrast with the reactivity of the simplest CI ($H_2COO$) and the earlier observation of an extensive reaction network with up

to four $H_2COO$ sequential addition (*Phys. Chem. Chem. Phys.,* **2019,** *21, 7341-7357*). Experimental photoionization efficiency scans recorded at 300 K and 425 K and *ab initio* threshold energy calculation lead to identification and quantification of previously elusive intermediates, such as ketohydroperoxide and hydroperoxide species. Specifically, the $C_4H_8 + O_3$ adduct is identified as a ketohydroperoxide (KHP, 3-hydroperoxybutan-2-one, $CH_3C(=O)CH(CH_3)OOH$), while hydroxyacetaldehyde (glycolaldehyde, $HCOCH_2OH$) formation is attributed to unimolecular isomerization of the CIs. Other hydroperoxide species such as methyl hydroperoxide ($CH_3OOH$), ethyl hydroperoxide ($C_2H_5OOH$), butyl hydroperoxide (OOH), hydroperoxyl acetaldehyde ($HOOCH_2CHO$), hydroxyethyl hydroperoxide ($CH_3CH(OH)OOH$), but-1-enyl-3-hydroperoxide, and 4-hydroxy-3-methylpentan-2-one ($HOCH(CH_3)CH(CH_3)C(=O)CH_3$) are also identified. Detection of additional oxygenated species such as methanol, ethanol, ketene, and aldehydes, suggest multiple active oxidation routes. These results provide additional evidence that CIs are key intermediates of the ozone-unsaturated hydrocarbon reactions providing critical inputs for improved kinetics models.

* Author to whom correspondence should be addressed. E-mail: denisia.popolan-vaida@ucf.edu, Tel: 407-823-1537.

## 1. Introduction

Carbonyl oxides, commonly known as Criegee intermediates (CIs), are important reactive intermediate species generated in the ozonolysis of unsaturated organic compounds in the atmosphere.[1] Their formation is attributed to ring-opening of primary ozonides (POZs) formed by the 1,3-cycloaddition of ozone across the olefinic bond, which subsequently decomposes to a carbonyl moiety and a carbonyl oxide, the CI.[1-3] The CIs are formed with a wide distribution of excess vibrational energy and can either undergo unimolecular isomerization or decomposition reactions often leading to the formation of OH radicals, or be collisionally stabilized, forming stabilized CIs.[3-4] The fate of CIs is essential and determines the products of the ozonolysis reaction and the impact of this reaction. For instance, in atmospheric chemistry, CIs play a key role in controlling the atmospheric budget of hydroxyl radical (OH)[5-8] and secondary organic aerosols.[3] CIs have fascinating oxidation properties and can react with species like $H_2O$,[9-12] $NO_2$,[13-14] $SO_2$,[13-17] $NH_3$,[18-19] organic acids,[20-21] aldehydes,[22-24] and alcohols[25-30] in the atmosphere with important implications for atmospheric kinetic models. The rate of some of these reactions has been found to strongly depend on the structure of CIs.[31] For instance, due to the double bond character of the CO bond, acetaldehyde oxide CI, $CH_3CHOO$, exists in two conformers, *syn* and *anti*, which have been reported to have different chemical behavior. While *syn*-$CH_3CHOO$ follows a fast thermal decomposition pathway that leads to the OH radicals formation via vinyl hydroperoxide decomposition, *anti*-$CH_3CHOO$ has been reported to rapidly react with atmospheric water vapors and forms a hydroxyl hydroperoxide.[32] Despite recent success exploring the chemical rate of individual CI reactions and their potential impact on atmospheric composition, the role of CIs in the formation of secondary organic aerosols is not completely understood, and only a few studies

reported the formation of oligomeric species composed of $CH_2OO$ CI units formed during the ozonolysis of ethylene.[31, 33]

Alkene-ozone reactions have also been the topic of significant interest in fundamental low-temperature combustion studies.[34-36] In ignition chemistry, the formation of reactive radicals such as OH, formed as a result of CIs unimolecular decomposition, may accelerate ignition while the formation of closed shell species tends to inhibit ignition. Recent work has shown that plasma-assisted combustion is a promising approach toward lowering emission and increasing efficiency of internal combustion engines.[35-36] Ozone is one of the reactive species produced in plasma that led to the enhancement of the combustion processes. However, the majority of the combustion systems operate at elevated pressure condition. The elevated pressures induce plasma instability and collisional stabilization of the discharge complicating the process of generating uniform large volume of plasma.[34] To bypass this problem, strategies like ozone assisted combustion have been proposed. Ozone can be efficiently produced under high pressure condition and has a long enough lifetime that allows its transport from the production source to the combustion chambers. Therefore, ozonolysis reactions could initiate fuel oxidation/dissociation far-off upstream of the combustion chamber, at temperature well below the dissociative limit of ozone, that will change the molecular structures (compositions) of reactants. It can potentially change both kinetic and transport properties of the reactants, therefore affecting the ignition characteristics.[36] However, there are still a lot of uncertainties regarding a fundamental understanding of $O_3$ assisted combustion, especially when ozonolysis reactions are the dominant pathways. Understanding the kinetic enhancement facilitated by ozone will allow for optimization of the current technologies to further reduce soot/$NO_x$ formation and increase efficiency.

In this work, the reaction network of acetaldehyde oxide CI ($CH_3CHOO$) is investigated following the ozonolysis of *trans*-2-butene. The ozonolysis of *trans*-2-butene proceeds with the initial formation of the primary ozonide (POZ) by 1,3 polar addition across the double bound of the *trans*-2-butene, forming a 1,2,3-trioxolane species (see Figure 1). Once formed, the POZ can either isomerize to a ketohydroperoxide (3-hydroperoxybutan-2-one, $CH_3C(=O)CH(CH_3)OOH$ - the KHP), or decompose into acetaldehyde and a vibrationally excited CI. The energy-rich CI and the acetaldehyde may recombine to form a secondary ozonide (SOZ, 1,2,4-trioxolane), undergo collisional stabilization and further react to form a range of products, or decompose into radicals and products (cf. Figure 1).

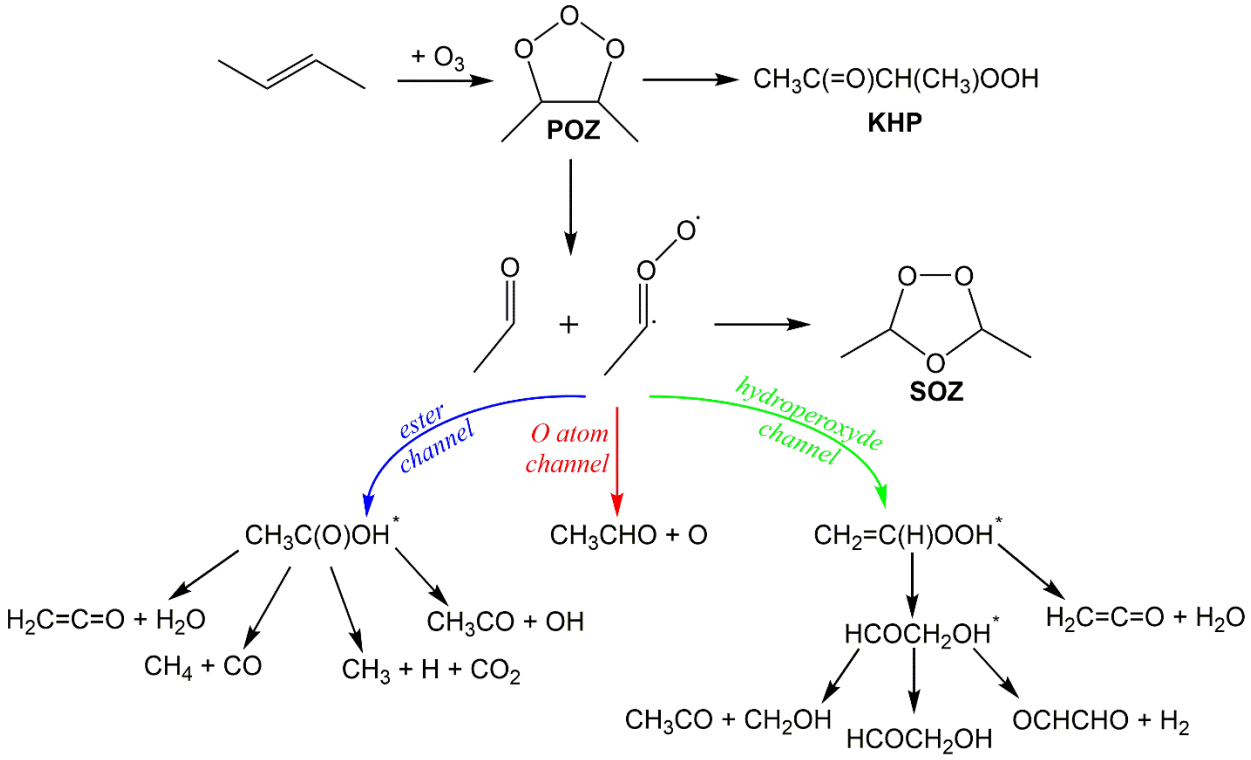


***Figure 1.*** *Trans-2-butene ozonolysis reaction pathway with major intermediate species. The species marked by an asterisk correspond to a highly excited, chemically activated state that can undergo funder unimolecular reactions, such as isomerization or decomposition.*

The unimolecular decomposition of CI has been described to proceed through three reaction channels: (i) ester channel, (ii) O-atom channel, and (iii) hydroperoxide channel (see Figure 1). Unique indicators for each channel, e.g. methane ($CH_4$) for the ester channel, diacetyl ($CH_3COCOCH_3$) for the O-atom channel, and glyoxal (OCHCHO) for the hydroperoxide channel, have been used in the literature to estimate a lower limit for the relative importance of each channel.[37]

The reaction of *trans*-2-butene has been investigated before under a variety of experimental conditions. Low-pressure (4-8 torr) ozonolysis reaction of *trans*-2-butene has been investigated by Martinez et al. using a photoionization mass spectrometer coupled to a stirred flow reactor.[38] The products reported in this study correspond to (i) a POZ split to a $C_m$ oxoalkane (aldehydes or ketones) and a CI, (ii) competing loss processes of the CI, i.e. unimolecular decomposition *vs*. CI reactions (such as SOZ formation), and (iii) secondary alkene chemistry involving OH and other free radical products formed as a result of the unimolecular decomposition of the CI.

A stopped-flow reactor in conjunction with photoionization mass spectrometry has also been used to investigate the reaction of *trans*-2-butene with ozone at 294 K and 530 Pa.[37] This study provides important information about the fate of CIs indicating that the mechanism of alkyl-substituted alkenes with ozone needs to account for additional reaction channels, such as ester, hydroperoxide and O atom channels, corresponding to CIs unimolecular decomposition/isomerization. Other studies investigated the mechanism of *trans*-2-butene reaction with ozone and the OH radical production in the presence and absence of an OH radical scavenger.[39-41] However, a complete description of the CI reaction network is currently lacking.

To extend our knowledge of the CI reaction network, a jet-stirred reactor equipped with molecular beam sampling capabilities in conjunction with high-resolution mass spectrometry and

tunable synchrotron radiation from the Advanced Light Source in Berkeley is used in this work to investigate the ozone-assisted oxidation reaction of *trans*-2-butene, by monitoring the reaction at atmospheric pressure over a range of temperatures between 300 and 900 K. This experimental arrangement in conjunction with *ab initio* threshold energy calculations facilitated the detection, identification and quantification of several reactive intermediates, such as ketohydroperoxide (KHP) and hydroperoxide species. The results presented here inform future developments of more detailed chemical descriptions of the ozone-assisted oxidation of alkenes.

## 2. Methodology

### 2.1 Experimental approach

The reaction of *trans*-2-butene with ozone is investigated over a broad range of temperatures between 300 and 900 K at a constant pressure of 0.92 atm (700 Torr), and an equivalence ratio of 0.5 (with a mixture of 1% *trans*-2-butene, 12% $O_2$, and 87% Ar), respectively. The ozone concentration was kept constant at a value of 1000 ppm during all measurements presented in this study. The product distribution was measured at various reaction times between 1 and 4 s. The data reported here is collected at a reaction time of 1.3 s for which the important intermediate species targeted in this study have the highest intensity.

The experimental setup employed in the present study consists of a jet-stirred reactor (JSR) system, a sampling system, and an analysis system. Details concerning the experimental technique used in these investigations are given elsewhere.[42] Briefly, the JSR is a custom-made fused silica sphere with a diameter of 4 cm and a volume of about 33.5 $cm^3$. It has four injectors located in the equatorial plane of the reactor oriented in opposite directions in order to achieve stirring in the whole reactor volume of the admitted reactants. It is based on the design by Dagaut et al.,[43] which

was slightly modified to accommodate direct sampling into a high-resolution ($m/\Delta m \approx 4000$) time-of-flight molecular beam mass spectrometer (TOF-MBMS). The JSR is preceded by a quartz annular preheating zone in which the gases are heated up to the desired temperature before entering the reactor. The necessity of the preheating region was proven by Azay and Côme,[44] which measured big temperature gradients in a continuous flow stirred reactor with no pre-heating of the gases. Heating of the gas flow in this region is achieved by means of an Inconel heating resistor (Thermocoax). The flow rates of *trans*-2-butene, oxidizers ($O_3$ and $O_2$), and Ar are regulated by calibrated MKS mass-flow controllers, while the fuel and oxidizer are kept separate in the concentric quartz tubes of the preheating zone prior to mixing at the entrance of the JSR. A fraction of the oxygen stream is sent into an ozone generator (Oriel) to produce controlled amounts of $O_3$. A 70 cm quartz absorption cell in conjunction with a helium neon UV calibrated lamp and an Ocean Optics spectrometer are used to monitor the concentration of $O_3$ just prior to the preheating zone at a wavelength of 312.57 nm, using the known ozone-adsorption cross section.[45]

The JSR exhaust is coupled to the TOF-MBMS through a quartz cone-like nozzle, with a 40° cone angle and a ~50 μm orifice diameter at the tip. The temperature inside of the reactor is regulated by a proportional–integral–derivative (PID) controlled tube furnace and monitored by means of an Inconel coated type K thermocouple (Thermocoax) placed in the proximity of the sampling conical nozzle. The reactor temperature is measured with an uncertainty of ± 20 K that is in part attributed to the cooling effect of the sampling nozzle. Previous experiments performed to test the reactor temperature homogeneity, by moving the thermocouple along the center line of the reactor, revealed a variation of only ± 5 K for dilution levels as low as 80% Ar and residence times up to 4 s, proving the temperature homogeneity of the reactor.

The TOF-MBMS employs vacuum ultraviolet (VUV) photons from the Chemical Dynamics Beamline of the Advanced Light Source[46-47] to measure photoionization spectra of product species. The synchrotron VUV radiation provides high photon flux ($10^{14}$ photons/s) and narrow bandwidth energy photons (E/ΔE(fwhm) ≈ 250-400) from 7.4 eV to 30 eV. The narrow bandwidth and the tunability allow for near-threshold ionization, which reduces fragmentation and simplify the interpretation of the mass spectra. In addition, the tunability of the synchrotron radiation enables isomer resolved species identification and quantification based on the comparison of the recorded photoionization spectra with the absolute photoionization spectra of individual isomeric species.

The conversion of the mass spectra signal to absolute mole fraction of the individual species is performed according to a well-developed procedure used for flame-sampling mass spectrometry experiments.[48-49] According to this procedure the signal S for a given m/z ratio and energy is related to the mole fraction $x_i$ by the following equation:

$$S_i(E) = x_i \cdot \varphi \cdot \mathrm{SW} \cdot \mathrm{D}(M_i) \cdot c \cdot \mathrm{FKT}(T) \cdot \sigma_i(E) \quad (1)$$

where $\varphi$ is the number of photons (measured by means of a calibrated photodiode), SW is the number of accumulated mass spectra (sweeps), $\mathrm{D}(M_i)$ is the mass discrimination factor for species $i$ (determined from the calibration measurements), $c$ is an instrumental factor, FKT(T) is a temperature-dependent sampling function, while $\sigma_i(E)$ is the absolute photoionization cross section, which is both molecule and energy dependent. The FKT can be determined as $c \cdot \mathrm{FKT}(T)$ assuming that the concentration of argon is known.

Temperature scans are recorded in 25 - 50 K increments at photon energies of 9.5 eV, 10.0 eV, 10.5 eV, 11.0 eV, 11.5 eV, 12.5 eV, 14. 35 eV, 16.2 eV, and 16.65 eV in a temperature range from 300 to 900 K. Photoionization efficiency curves are recorded at 300 K, 425 K and 500 K in the

presence of ozone and at 800 K in the absence of ozone, as $O_3$ thermally decomposes around 600 K.

### 2.2 Theoretical approach

The ionization energies of many key intermediates formed in the ozonolysis of *trans*-2-butene are unknown which hinders their identification. An automated approach is implemented in this study to systematically explore conformeric structures of key intermediates and to compute up to $\sim 3^{N_{torsion}}$ locally adiabatic ionization energies,[42] where $N_{torsion}$ is the number of rotatable bonds. The cheminformatics tool, Open Babel,[50-51] was used to generate initial geometry guesses from the chemical structure. Candidate conformers were then generated by spinning all rotatable bonds by fixed step sizes. A step size of 120° was used for torsions with $sp^3$ hybridization for both central atoms (the majority of cases), and 60° step sizes were used otherwise (e.g., for torsions where one of the rotatable groups is the –CHO group). Each candidate structure was minimized first using Open Babel's automated conformer generating strategy ''confab'' and then using M06-2X/cc-pVDZ. The structures were checked for duplicates, including mirror images, and higher-level ionization energies were computed for the unique conformers using the ~CCSD(T)/CBS//M06-2X/cc-pVTZ level of theory, where ~CCSD(T)/CBS indicates that the complete basis set limit correction to CCSD(T)/cc-pVTZ was estimated using MP2 and the cc-pVTZ and cc-pVQZ basis sets, as employed elsewhere.[42, 52] The locally adiabatic ionization energy was computed for each conformer. Often, the locally adiabatic ionization energies are in close agreement with one another and with the global adiabatic ionization energy, and unless otherwise indicated the values given below are the locally adiabatic ionization energies for the lowest-energy conformer. The consideration of higher-energy conformers is sometimes useful for interpreting the observed PIE

curves, as noted below. As discussed, and demonstrated in previous publications,[49, 53-56] the calculated adiabatic ionization energies are often good predictors of the experimental ionization thresholds (typically within ~0.1 eV) and are thus often sufficient for species identification. Often, the locally adiabatic ionization energies are in close agreement with one another and with the global adiabatic ionization energy, as is the case for all of the calculated ionization energies reported here.

## 3. Results and Discussion

### *3.1 Ozone assisted oxidation reaction of trans-2-butene*

The presence of ozone initiates the oxidation of *trans*-2-butene at room temperature, resulting in a low temperature combustion (LTC) region in which approximately 25% of the *trans*-2-butene signal is consumed at 500 K (see Figure S1 in Supplementary Information). Above 500 K, a negative temperature coefficient (NTC) region is formed that corresponds with a decrease in reactivity with increasing temperature. This might be explained as a result of the high-temperature thermal decomposition of ozone triggering a decrease of the *trans*-2-butene consumption via low temperature *trans*-2-butene oxidation pathways. This is in agreement with the data reported by Zhao et al. who observed ozone thermally decomposing by 600 K.[57] The transition from the LTC to the flat intermediate region of 600 K also corresponds to a complete thermal decomposition of ozone. Above 600 K the *trans*-2-butene signal starts decreasing again, as opposed to the non-ozone experiments where the oxidation reaction was observed for temperatures above 950 K. At 900 K only about 4% of the initial *trans*-2-butene signal is left. This consumption might be attributed to the O atom reactions, formed as a result of $O_3$ thermal decomposition.

The product distribution in the temperature region below 600 K is characteristic of the ozonolysis reactions. However, once initiated by ozone, the reaction mechanism in the low-temperature region is also dominated by low-temperature oxidation chemistry that includes the formation of hydroperoxy molecules. Alkyl hydroperoxide species like methyl hydroperoxide ($CH_3OOH$), ethyl hydroperoxide ($C_2H_5OOH$), and butyl hydroperoxide ($C_4H_9OOH$), typically identified as low-temperature oxidation intermediates, are detected in our experiment in a temperature range between 300 K to 550 K. The formation of these hydroperoxy species has been also observed in the ozonolysis of ethylene.[52] The PIE curves of methyl, ethyl, and butyl hydroperoxides detected in our experiments are shown in Figure S2, while the mole fraction temperature profiles of $CH_3OOH$ and $C_2H_5OOH$ concentrations are displayed in Figure S3. In addition, species like hydroperoxy acetaldehyde and but-1-enyl-3-hydroperoxide are also identified under our experimental conditions (see Figure S4).

Due to the complexity of the reaction mechanism that involves contributions from both $O_3$ and $O_2$ chemistry, it is difficult to infer definitive formation pathways for the detected hydroperoxide species. However, according to the typical low-temperature oxidation mechanism,[58] the alkyl hydroperoxides (ROOH) are expected to be formed in a sequential mechanism that involves the formation of ROO· radical and its subsequent reaction with $\cdot HO_2$. Consequently, $C_4H_9OOH$ is expected to be formed via the $C_4H_9OO + HO_2$ reaction, with $C_4H_9$ originating from H-addition to *trans*-2-butene. The formation of but-1-enyl-3-hydroperoxide can be attributed to the combination of alkenyl radical, formed by H abstraction from *trans*-2-butene, with an HOO· radical, and the bimolecular reaction of HOO· with ROO·, which is produced from the $O_2$ addition to the alkenyl radical. The detection of these hydroperoxides in our study confirms the necessity of including them in mechanisms for ozone-assisted oxidation of alkenes.

Above 600 K, in the intermediate temperature region (600-800 K), the oxidation rection is initiated by O atom and only a few species like propene ($C_3H_6$), 1,3-butadiene ($C_4H_6$), 2-butenal ($C_4H_6O$), diacetyl ($C_4H_6O_2$) are detected and identified based on photoionization efficiency scans. The products observed at rection temperatures above 800 K are similar to the once reported in the literature for the reaction of *trans*-2-butene reaction with $O_2$.[59-60] In an ozone-free environment, *trans*-2-butene has been reported to undergo oxidation reaction at temperatures above 925 K. As ozone thermally decomposes at temperatures above 600 K, atomic and molecular oxygen are the only oxidants at reactor temperatures above 600 K. The presence of atomic oxygen appears to initiate the high-temperature oxidation reaction already at 800 K, which is about 150 K below the temperature where Fenard et al. observed the first oxidation products when only $O_2$ was present in the reactor. As the product distribution at 800 K is indicative for a mechanism similar to the one reported by Fenard et al.,[59-60] this study focuses on the temperature region between 300 K and 600 K where the oxidation reactions are dominated by ozone chemistry. A table that summarizes all the reaction products identified in our study is available in the Supplementary Material (see Table S1). Due to the lack of reaction rate constants for many important elementary steps in the mechanism of ozone assisted oxidation of trans-2-butene, no modeling was performed for this reaction.

### *3.2. Evidence for the formation of acetaldehyde oxide*

Following the oxidation scheme displayed in Figure 1, the initial step in the *trans*-2-butene ozonolysis reaction involves the formation of a primary ozonide, POZ (1,2,3-trioxolane, *m/z* = 104.047) by $O_3$ addition across the double bound of *trans*-2-butene. Once formed, POZ can either isomerize into a ketohydroperoxide (KHP, 3-hydroperoxybutan-2-one, $CH_3C(=O)CH(CH_3)OOH$) or decompose into acetaldehyde and a vibrationally excited CI. Subsequently, the energy-rich CI and the acetaldehyde may recombine to form a SOZ (1,2,4-trioxolane, *m/z* = 104.047).

Consequently, the signal recorded at *m/z* = 104.047 in the mass spectrum could be attributed to any of these species, POZ, KHP, or SOZ, respectively.

Figure 2(a) displays the photoionization efficiency (PIE) curve of *m/z* = 104.047 ($C_4H_8O_3$) recorded at T = 300 K. Calculated adiabatic ionization energies of the POZ and SOZ

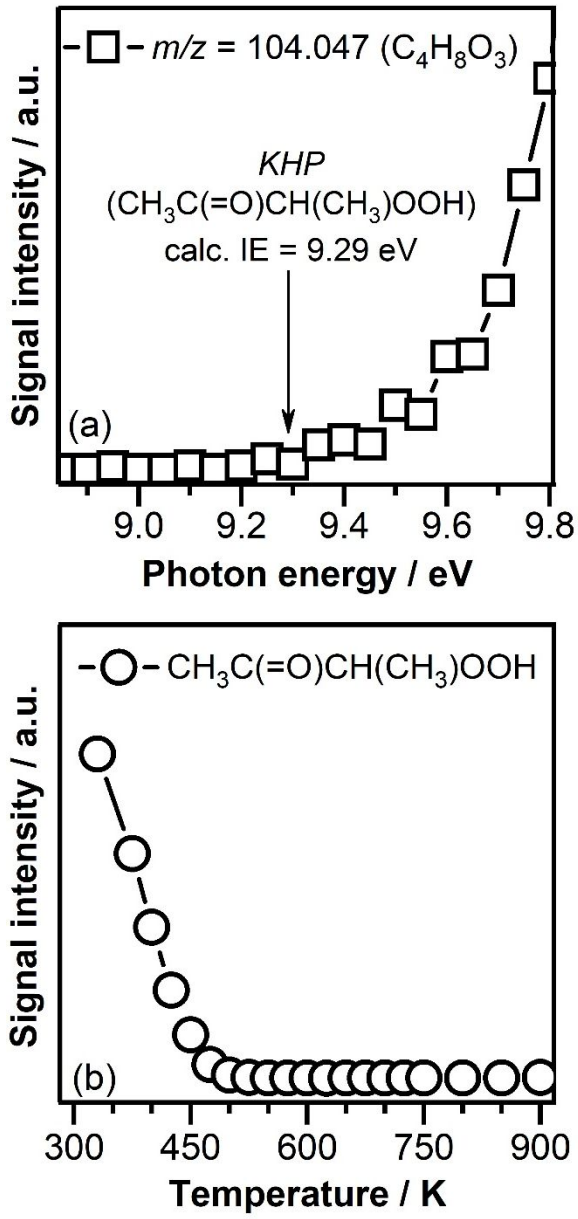


***Figure 2:*** *(a) Photoionization efficiency curve of m/z = 104.047 ($C_4H_8O_3$) recorder at T = 300 K. The calculated adiabatic ionization energies KHP is indicated by the arrow. (b) $C_4H_8O_3$ signal intensity as a function of temperature recorded at a photon energy of 10.00 eV.*

are 9.17 eV (for *trans*-POZ), 9.11 eV (for *cis*-POZ), 9.23 eV (for *trans*-SOZ), and 9.10 eV (for *cis*-SOZ), respectively. As can be seen in Figure 2(a), no signal corresponding to POZ and SOZ is detected under our experimental conditions as no signal is present in the energy range where those species are expected to be ionized. However, the calculated ionization energy of the lowest energy conformer of KHP (3-hydroperoxybutan-2-one, $CH_3C(=O)CH(CH_3)OOH$) of 9.29 eV matches the experimentally observed threshold. Therefore, the signal recorded at $m/z$ = 104.047 is attributed to the presence of 3-hydroperoxybutan-2-one. This observation is consistent with the detection of the KHP in similar ozonolysis experiments of ethylene.[52]

Figure 2(b) shows the evolution of the signal recorded at $m/z$ = 104.047 as a function of temperature. It is well established that alkenes react with ozone at already room temperature. The signal observed at $m/z$ = 104.047 monotonically decreases with increasing temperature. The signal approaches the detection limit at temperatures above 500 K, following the ozone trend. The decrease in the $C_4H_8O_3$ signal with increasing temperature might be attributed to the thermal decomposition of KHP as well as to an increase in the decomposition rate of ozone that results in an overall decreasing concentration of the initial POZ and consequently of the KHP.

As mentioned above, the decomposition of POZ also leads to the formation of another important intermediate species, the CI (acetaldehyde oxide, $CH_3CHOO$), expected at $m/z$ = 60.021. $CH_3CHOO$ is recognized to be the smallest CI that has two conformers (*anti*- and *syn*-CI) and also the smallest to have a hydroperoxide isomer (vinylhydroperoxide). The calculated adiabatic ionization energy (AIE) of both CIs and vinylhydroperoxide have values below 9.6 eV.[14, 61-62]

Figure 3(a) displays the PIE scan of $m/z$ = 60.021 signal recorded at 300 K. As can be seen in Figure 3(a), the ionization threshold is observed at a photon energy of 9.90 ± 0.05 eV. In addition, the signal presents a sharp rise near 10.65 ± 0.05 eV. No measurable concentration of CIs or their

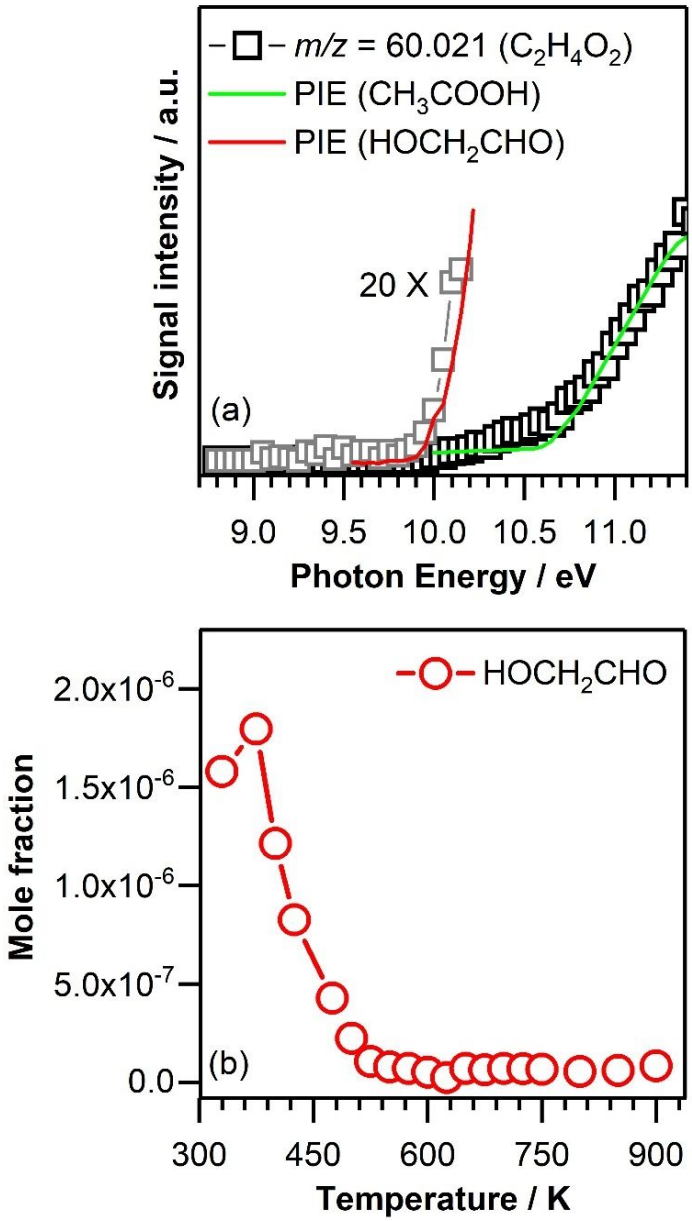


***Figure 3:*** *(a) Photoionization energy scan of m/z = 60.021 ($C_2H_4O_2$) signal recorded at T = 300 K (open squares). The glycolaldehyde PIE curve (red curve) reported by Ellison et al.[63] matches the 9.5 to 10.2 eV region of the PIE spectra recorded in our experiment. Green curve corresponds to the acetic acid PIE curve.[64] (b) $C_2H_4O_2$ mole fraction as a function of temperature recorded at a photon energy of 10.50 eV.*

hydroperoxide isomer (vinylhydroperoxide) was detected under our experimental conditions, even with a similar PIE scan at 425 K, as no signal was detected in the energy range where these species

are expected to be ionized. Concentrations below the instrument's detection threshold (1 ppm) suggest rapid reactions, which might lead to CIs depletion due to the low activation energy for reaction. Despite the fact that acetaldehyde oxide is not detected under our experimental conditions, acetaldehyde oxide formation is indirectly confirmed via the detection of species like glycolaldehyde ($HCOCH_2OH$) and glyoxal (HCOCHO).

At $m/z$ = 60.021, products like glycolaldehyde, 1,2-dioxetane, acetic acid, and methyl formate can also contribute to the mass spectra signal besides the CI. The observed onset at 9.95 ± 0.05 eV of the $m/z$ = 60.021 signal in Figure 3 (a) is in agreement with the ionization threshold of 9.98 eV calculated for glycolaldehyde.[52] In addition, the PIE spectra of the glycolaldehyde reported in the literature[63] fits well the 9.5 to 10.2 eV region of the PIE spectra recorded in our experiment (see Figure 3(a)). According to the ozonolysis scheme shown in Figure 1, glycolaldehyde is formed via the hydroperoxide channel as a result of unimolecular isomerization of CIs. Other products characteristic to the hydroperoxide channel, such as glyoxal or ketene are also detected under our experimental conditions.

The signal increase above 10.65 ± 0.05 eV observed in Figure 3(a) correlates with the presence of acetic acid (IE = 10.65 eV[64]). While no evidence for 1,2-dioxetane was found (AIE = 9.35 eV[42]), we cannot exclude the presence of small amounts of methyl formate (IE = 10.83 eV[65]).

Figure 3(b) displays the temperature dependent mole fraction profile of the glycolaldehyde collected at an ionization energy of 10.5 eV, which is slightly above the ionization energy of glycolaldehyde and below the ionization energy of other possible isomers that contribute to the signal recorded at $m/z$ = 60.021. The mole fraction of glycolaldehyde is based on a photoionization cross section of 6.1 Mb at 10.5 eV reported in the literature.[52] As can be seen in Figure 3(b) the signal monotonically decreases with increasing temperature and vanishes around 575 K.

As mentioned above, the lack of CIs signal in the recorder PIE might be due to the fact that CIs are formed with an excess of vibrational energy, and a fraction of CIs can undergo unimolecular decomposition, while the remaining fraction of vibrationally stabilized CIs further reacted in the timescale of our experiment. Our experimental results indicated both the presence of reaction products formed as a result of unimolecular decomposition/isomerization of CIs and reaction products formed as a result of the reaction of the vibrationally stabilized CIs with species like *trans*-2-butene, water, formaldehyde, and formic acid.

### *3.3 Unimolecular decomposition of CIs*

An important fraction of vibrationally excited CIs formed during the *trans*-2-butene ozonolysis reaction have been reported to decompose unimolecularly.[37-38] As described above (see Fig. 1), methane, diacetyl, and glyoxal, which are identified in our experiment, are unique indicators for the various CI decomposition channels. The signal intensity of glyoxal and diacetyl as a function of temperature are shown in Figure S5 and Figure S6, respectively. Diacetyl, which is the O-atom channel fingerprint, has been reported to form as a result of O + *trans*-2-butene reaction in the presence of excess $O_2$.[66] Its formation mechanism explains why a very small signal corresponding to its presence is detected in our experiment also at temperature where $O_3$ thermally decomposes (see Figure S5 in Supplementary Information) to atomic and molecular oxygen. In addition to methane, diacetyl, and glyoxal, species like ketene ($CH_2CO$) and methanol ($CH_3OH$) characteristic to both ester and hydroperoxide channels are identified as well. However, the lack of ionization cross section of both diacetyl and glyoxal precludes an accurate quantification of the relative importance of CIs unimolecular decomposition channels.

### *3.4 Reactions of stabilized CIs*

A fraction of excited CIs has been found to vibrationally stabilize under our experimental conditions and further reacts with other species. Products detected in our experiment correspond to CIs reaction with species like *trans*-2-butene, water, formic acid, formaldehyde, and methanol.

*Reaction of CIs with trans-2-butene*

The CI-alkene reaction was first observed by Story at al., who investigated the ozonolysis reaction of tetramethylethylene.[67] Rousso et al. studied the ozonolysis of ethylene and hypothesized that the observed allyl hydroperoxide ($C_2H_3CH_2OOH$) and possibly 3-hydroxypropanal are products of the reaction of $C_2H_4$ with $CH_2OO$.[33] Reactions of CIs with alkenes proceed in a similar manner as the isoelectronic reaction of $O_3$ with alkenes by 1,3-dipolar cycloaddition of $O_3$ across the C=C to form a 1,2-dioxolane. Vereecken et al. calculated the stationary points at the M06-2X/aVTZ and CCSD(T)/aVTZ//M06-2X levels of theory for several reactions of CIs with alkenes including the reaction of *syn*-$CH_3CHOO$ and *anti*-$CH_3CHOO$ with *trans*-2-butene.[68] The *syn*-$CH_3CHOO$ have been reported to be much less reactive than *anti*-$CH_3CHOO$. Moreover, the $CH_3CHOO$ addition to *trans*-2-butene results in the formation of a cyclic peroxide (cyc-$CH(CH_3)CH(CH_3)CH(CH_3)OO$-), that is considerably more stable than the corresponding POZ:

$$CH_3CHOO + C_4H_8 \leftrightarrows \text{cyc-}CH(CH_3)CH(CH_3)CH(CH_3)OO\text{-} \quad \text{(R1)}$$

The product mass spectrum recorded at a temperature of 300 K displays a signal at *m/z* = 116.083 ($C_6H_{12}O_2$) that points toward the reaction of CI with *trans*-2-butene. The corresponding PIE curve is displayed in Figure 4. As can be seen in Figure 4, the ionization threshold of the signal recorded at *m/z* = 116.083 appears to be around 9.35 ± 0.05 eV. As mentioned above, Vereecken et al. predicted that the CI + alkene reaction lead to the formation of a cyclic peroxide.[68] However,

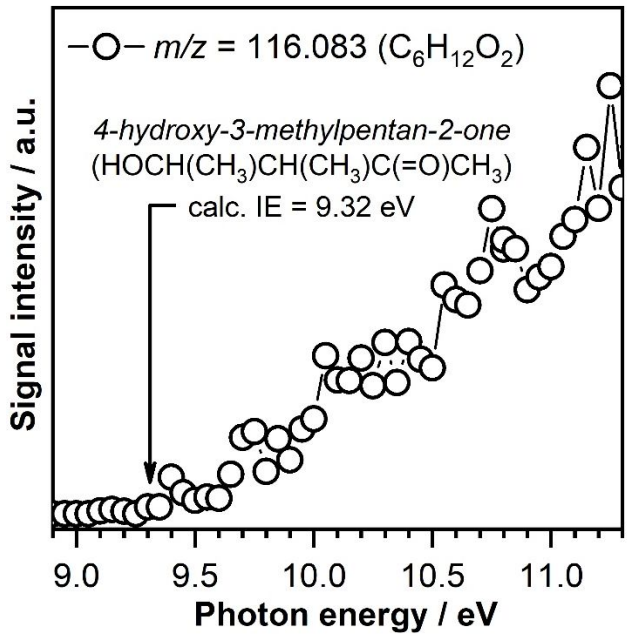


***Figure 4.*** *Photoionization energy scan from 9.00 eV to 11.25 eV for m/z = 116.08 ($C_6H_{12}O_2$) signal recorded at 300 K. The ionization threshold is observed at a photon energy of 9.32 ± 0.05 eV. The arrow indicates the IE calculated in this study.*

the adiabatic ionization energy calculated in this study for cyclic peroxide is 8.62 eV, which is smaller than the experimentally observed ionization threshold of about 9.35 ± 0.05 eV. Therefore, we can exclude the formation of considerable amount of cyclic product under our experimental conditions.

Earlier work by Pfeifer et al. revealed that the primary ozonide can undergo ring opening *via* a diradical structure to form a ketohydroperoxide.[69] A similar reaction might be possible in the case of 1,2-dioxolane [cyc-$CH(CH_3)CH(CH_3)CH(CH_3)OO$], formed as a result of the reaction of CI with *trans*-2-butene, resulting in the formation of 4-hydroxy-3-methylpentan-2-one [$HOCH(CH_3)CH(CH_3)C(=O)CH_3$]. The adiabatic ionization energy calculated in this study for 4-hydroxy-3-methylpentan-2-one of 9.32 eV matches the experimental ionization threshold observed at 9.35 ± 0.05 eV (see Figure 4). The decomposition of 1,2-dioxolane to form an olefinic

hydroperoxide was also considered in this study. Olefinic hydroperoxides, which are species with a C=C double bond and a hydroperoxide group, have been recently identified as important intermediates in low-temperature oxidation chemistry of hydrocarbons.[70-71] The adiabatic ionization energy of 8.72 eV calculated for 4-hydroperoxy-3-methylpent-1-ene lays well below the experimental ionization threshold observed at 9.35 ± 0.05 eV (see Figure 4). In conclusion, the signal detected at m/z = 116.083 is consistent with the presence of 4-hydroxy-3-methylpentan-2-one, while within the detection limit of our experiment no evidences were found for the formation of either cyclic peroxide [cyc-$CH(CH_3)CH(CH_3)CH(CH_3)OO$] or olefinic hydroperoxide, 4-hydroperoxy-3-methylpent-1-ene [$HOOCH(CH_3)C(CH_3)=CHCH_3$]. This observation is in large consistent with the observations of Rousso et al.[33] Further sequential addition reaction of the $CH_3CHOO$ to the multi-functional products are not observed in our study.

*Reaction of CIs with water*

The reaction of CIs with water are recognized to dominate the tropospheric CIs removal.[72-73] The primary products formed in this reaction, i.e. hydroxyalkyl hydroperoxides are important trace atmospheric constituents acting as oxidants themselves or as reservoirs/sinks of $RO_2$ and $HO_x$ species.[74-75] The reactivity of larger CIs, such as $CH_3CHOO$, with water is expected to be controlled by the nature and location of substituents or by the conformations they adopt in the gas-phase.[10, 76] The reaction of *syn*-$CH_3CHOO$ and *anti*-$CH_3CHOO$ conformers has been already investigated, and the *anti*-$CH_3CHOO$ conformer was found to be substantially more reactive towards water than the *syn*- $CH_3CHOO$.[9-10, 14, 77-80] The reaction was found to lead to the formation of hydroxyethyl hydroperoxide products [HEHP, $CH_3CH(OH)OOH$]. The reaction begins with the

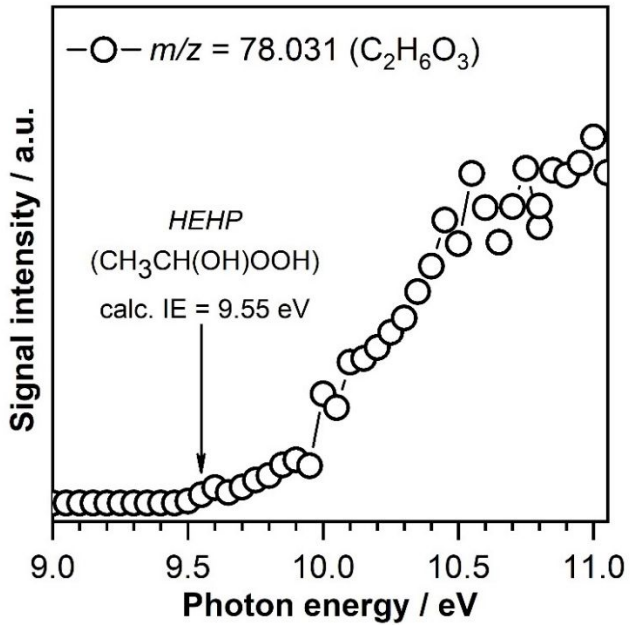


***Figure 5.*** *Photoionization energy scan from 9.00 to 11.05 eV for m/z = 78.031 ($C_2H_6O_3$). The ionization threshold is observed at a photon energy of 9.55 ± 0.05 eV. The arrow indicates the IE calculated in this study.*

formation of a pre-reactive hydrogen bonded complex by 1,3-dipolar cycloaddition of water to the CIs, followed by the formation of HEHP. This process involves the addition of the oxygen from the water molecule to the carbon atom of the carboxylic group of the CIs and the subsequent transfer of one hydrogen of water to the terminal oxygen atom of the CI.

$$CH_3\,CHOO + H_2O \leftrightarrows CH_3\,CH(OH)OOH \qquad \text{(R2)}$$

The mass spectrum recorded at a temperature of 300 K (not shown here) displays a peak at m/z = 78.032 ($C_2H_6O_3$). Figure 5 shows the PIE curve of $C_2H_6O_3$ signal recorded at a temperature of 300 K. The ionization threshold of the $C_2H_6O_3$ signal is observed at a photon energy of 9.55 ± 0.05 eV, while the signal presents a pronounced breakpoint near 10.2 ± 0.05 eV. Based on the excellent match between the experimentally observed and calculated ionization energy for the hydroxyethyl hydroperoxide, the signal at *m/z* = 78.032 is consisted with the presence of bifunctional HEHP.

The observed breakpoint near 10.2 ± 0.05 eV in the experimentally measured PIE curve (see Figure 6) might be attributed to a fragment formed as a result of dissociative ionization of hydroperoxyethyl formate (see details below).

*Reaction of CIs with formaldehyde*

The reaction of CIs with aldehydes are known to proceed by 1,3-dipolar cycloaddition of the carbonyl oxide to the -C(=O) double bound of aldehyde.[23] The reaction of formaldehyde with CIs is expected to proceed in a similar fashion as the acetaldehyde + CI reaction, and result in the formation of a secondary ozonide [cyc-$CH(CH_3)OOCH_2O$-].

$$CH_3CHOO + HCHO \leftrightarrows \text{cyc-}CH(CH_3)OOCH_2O- \quad \text{(R3)}$$

The adiabatic ionization energy of cyc-$CH(CH_3)OOCH_2O$- ozonide, calculated in this study at the same level of theory as described above, has a value of 9.41 eV. The experimental PIE recorded at $m/z$ = 90.031 ($C_3H_6O_3$) displayed in Figure 6 reveals a threshold for ionization near 9.40 ± 0.05 eV, which is consistent with the theoretically calculated IE value for cyc-$CH(CH_3)OOCH_2O$-. Therefore, part of the signal recorded at $m/z$ = 90.031 is attributed to the cyc-$CH(CH_3)OOCH_2O$-, which is the only cyclic intermediate identified in this study. The cyc-$CH(CH_3)OOCH_2O$- secondary ozonide can subsequently isomerize to hydroxymethyl acetate [HMA, $HOCH_2OC(CH_3)=O$] and 1-(hydroxymethoxy)ethan-1-ol [$HOCH(CH_3)OCHO$] via ring opening. The ionization energies of the hydroxymethyl acetate and 1-(hydroxymethoxy)ethan-1-ol are calculated to be 10.22 eV (with the lowest conformer appearing at 10.10 eV) and 10.46 eV (with conformers at 10.32 and 10.35 eV), respectively. The calculated ionization energy of HMA matches the observed breakpoint near 10.2 ± 0.05 eV in the experimentally measured PIE curve (see Figure 6). In addition, the calculated ionization energy of 1-(hydroxymethoxy)ethan-1-ol

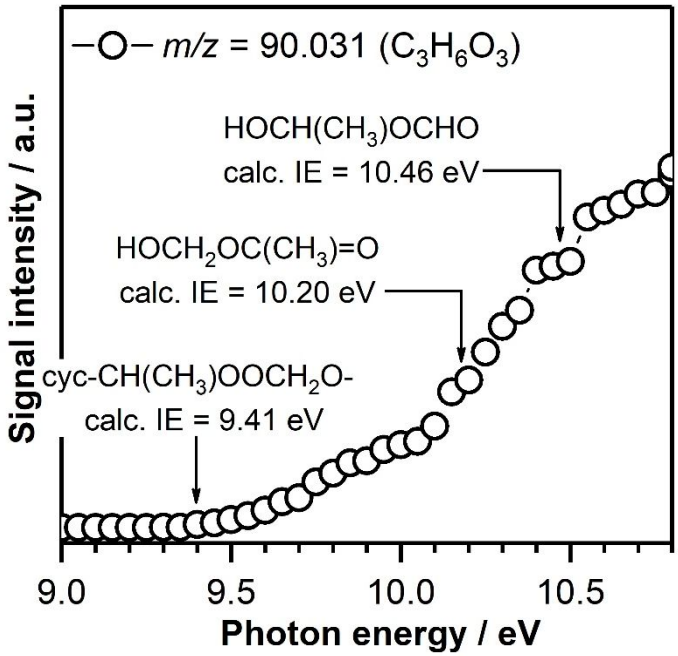


***Figure 6:*** *Photoionization energy scan from 9.00 eV to 11.3 eV for m/z = 90.031 ($C_3H_6O_3$). The ionization threshold is observed at a photon energy of 9.41 ± 0.05 eV. The breakpoints observed in the PIE around 10.15 eV and 10.50 eV suggest that additional species like $HOCH_2OC(CH_3)=O$ and $HOCH(CH_3)OCHO$ might contribute to the observed signal. The arrows indicate the IEs calculated in this study.*

appears to match the second breakpoint in the PIE curved observed at an ionization energy of about 10.5 ± 0.05 eV. The observed breakpoints in the PIE curve in Figure 6 does not necessarily indicate the presence of these species neither exclude the presence of other isomeric species.

*Reaction of CIs with formic acid*

The reaction of acetaldehyde oxide with formic acid is known to lead to the formation of hydroperoxyethyl formate (HPEF, $HOOCH(CH_3)OCHO$):

$$CH_3CHOO + HCOOH \leftrightarrows HOOCH(CH_3)OCHO \quad (R4)$$

A total of four different HPEF conformers (two for each syn- and anti-$CH_3CHOO$), differing in the position of the –C(O)H group over the OOH and $CH_3$ moieties, can be formed as a result of this reaction. The $CH_3CHOO$ + HCOOH reaction and the corresponding rate coefficients have been experimentally and theoretically investigated, but the detection of HPEF has been only recently reported.[81] This reaction has been also reported to lead to the formation of vinyl hydroperoxide via formic acid-catalyzed tautomerization of $CH_3CHOO$.[61]

A significant amount of formic acid is detected in our experiment, while its presence as a product of the reaction of *trans*-2-butene with ozone has been also reported in the literature.[38] However, no signal was detected under our experimental conditions at *m/z* = 106.026 that correspond to the mass of HPEF. A possible explanation for the lack of signal at *m/z* = 106.026 is that HPEF undergoes photodissociative ionization. This observation is in agreement with the results reported by Welz et al. who employed multiplexed photoionization mass spectrometry to investigate the reaction of two CIs ($CH_2OO$ and $CH_3CHOO$) with formic acid.[20] They attributed the lack of the signal at the parent masses of the CI-acid adducts to the photodissociative ionization of these adducts. In later studies, hydroperoxymethyl formate (HPMF), expected to be formed as a result of $CH_2OO$ + HCOOH reaction, has been reported to mainly undergo photodissociative ionization and its presence was unambiguously confirmed by the detection of a trace amount of the parent molecule, but mostly via the detection of $CH_4O_3$ photo-fragment whose appearance energy matched the calculated appearance energy of the $CH_4O_3$ fragment.[33, 42] Assuming a similar photodissociative ionization scenario as observed for HPMF, it is expected that part of the signal recorded at *m/z* = 78.032 might be due to $HOOCH(CH_3)OH^+$ photo-fragment of the HPEF cation ($HOOCH(CH_3)OCHO^+ \longrightarrow HOOCH(CH_3)OH^+ + CO$). Interestingly enough, the PIE curve recorded at *m/z* = 78.032 (see Figure 5) presents a break point around 10.00 ± 0.05 eV that indicates

the onset of an additional species that contributes to the recorded PIE signal apart from HEHP. To our knowledge, no information is available so far about either the ionization energy of HPEF or the appearance energy of its photo-fragments. Further work is necessary to characterize the ionization behaviors of HPEF. In contrast to the results presented by Liu at al.,[61] no vinyl hydroperoxide was observed within the detection limit of our experiment.

*Reaction of CIs with methanol*

Methanol ($CH_3OH$) is known as one of the most abundant oxygenated volatile organic compounds (OVOCs) in the atmosphere,[82-83] originating from terrestrial biogenic sources, of which tropical rainforests are among the largest.[84] The reactions of $CH_3OH$ with CIs is known to proceed by CIs insertion into the hydroxyl moiety of $CH_3OH$, similar to the reaction between CIs with water, to generate α-methoxyalkyl hydroperoxides, which are recognized as a potential source of OH radicals and OVOCs that promote the formation of secondary organic aerosols in the atmosphere.[25]

The reaction of $CH_3CHOO$ with $CH_3OH$ has been investigated by Lin et al.,[27] Chao et al.,[28] and Cabezas et al.[29] This reaction leads the formation of methoxyethyl hydroperoxide [$HOOCH(CH_3)OCH_3$, MEHP]:

$$CH_3CHOO + CH_3OH \leftrightarrows HOOCH(CH_3)OCH_3 \quad (R5)$$

In addition to the R5 reaction channel, the *syn*-$CH_3CHOO + CH_3OH$ reaction has been reported to have an additional pathway that can produce vinyl hydroperoxide ($CH_2$=CHOOH, VHP). None of the products expected to be formed via the reaction of $CH_3CHOO$ with methanol are directly observed at $m/z$ = 92.047 under our experimental conditions despite of the fact the methanol is present in considerable amount. A possible explanation for the lack of signal at $m/z$ = 92.047 corresponding to MEHP is that this product dissociates as a result of photodissociative ionization.

A possible photodissociation channel might be the loss of OOH group [$HOOCH(CH_3)OCH_3^+ \leftrightarrows CH(CH_3)OCH_3^+ + OOH$]. The recorded mass spectra present a signal at *m/z* = 59.049 which might be attributed to the $CH(CH_3)OCH_3^+$ photofragment. Figure 7 displays the $C_3H_7O$ (*m/z* = 59.049) signal intensity (a) as a function of photon energy and (b) as a function of temperature recorded at a photon energy of 10.00 eV. As can be seen in Figure 7(a) a signal is detected at *m/z* = 59.049 at a relatively low photon energy of 9.25 ± 0.05 eV, which is in agreement with our calculated ionization energy for MEHP of 9.30 eV. The observed $C_3H_7O$ signal increases with increasing temperature (see Figure 7(b)), reaches a maximum around 400 K, and subsequently decreases with increasing temperature, to vanish around 600 K, which corresponds to the temperature where $O_3$ thermally decomposes.

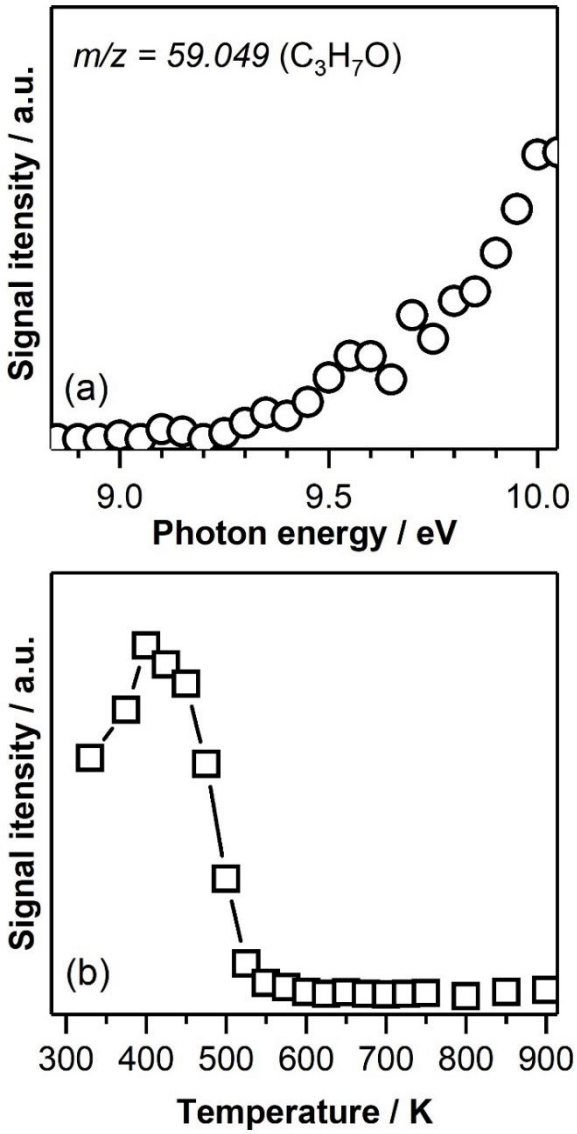


***Figure 7.*** *(a) Photoionization efficiency curve of m/z = 59.049 ($C_3H_7O$) recorder at T = 300 K. (b) $C_3H_7O$ signal intensity as a function of temperature recorded at a photon energy of 10.00 eV.*

The lack of signal at temperatures above 600 K indicated that this is a photofragment originating from a species that is produced as a result of $O_3$ reactions and support our hypothesis that this might be the MEHP photofragment. Finally, we note that HOO loss from the MEHP cation is calculated to be exothermic, further supporting this explanation.

## Conclusions

This study characterizes the reaction network of the second simplest CI, $CH_3CHOO$, by employing a jet-stirred reactor system in conjunction with photoionization TOF-MBMS. Key intermediate species are identified utilizing photoionization energy scans and when possible quantified using recently developed routines. Three distinct temperature-dependent kinetic regions are identified that correspond to (i) ozone assisted oxidation (< 600 K) dominated by ozone chemistry and CI reactions, (ii) intermediate temperature oxidation (600-800 K) initiated by O atoms, and (iii) high-temperature oxidation (> 800 K).

At temperatures below 600 K a network of uni- and bi- molecular CI reactions are identified, characterized by CIs decomposition/isomerization or addition to species like *trans*-2-butene, water, formaldehyde, formic acid, and methanol. Unlike the simplest CI ($CH_2OO$), no products corresponding to multiple $CH_3CHOO$ addition are observed in this study. Lack of direct detection of the Criegee intermediate suggests either fast reaction channels or that stabilization reactions of the activated complex are less important at raised temperatures. Experimental photoionization efficiency scans recorded at 300 K and 425 K in conjunction with *ab initio* threshold energy calculations lead to identification and quantification of previously elusive intermediates, such as ketohydroperoxide and hydroperoxide species. In the high-temperature region, little difference is identified between ozone and non-ozone cases due to radical quenching at the fixed temperature of the JSR. Identification and quantification of other oxidized species suggest multiple active oxidation routes. The results of this study help bridging the gap between atmospheric and flame chemistry studies.

## Acknowledgements

D.M.P.-V. gratefully acknowledges financial support provided by UCF through the "VPR Advancement of Early Career Researchers" program. A.R.C., N.T. and L.H.-R. acknowledge financial support provided by UCF Office of Undergraduate Research. N.H. and A.W.J. acknowledge support from the U.S. DOE, Office of Science, Office of Basic Energy Sciences. We gratefully acknowledge computing resources provided by Bebop, a high-performance computing cluster operated by the Laboratory Computing Resource Center at Argonne National Laboratory. Sandia National Laboratories is a multi-mission laboratory managed and operated by National Technology and Engineering Solutions of Sandia, LLC., a wholly owned subsidiary of Honeywell International, Inc., for the U.S. DOE National Nuclear Security Administration under contract DE-NA0003525. A.W.J. is supported by the Division of Chemical Sciences, Geosciences, and Biosciences, under Contract Number DE-AC02-06CH11357. The Advanced Light Source is supported by the Director, Office of Science, Office of Basic Energy Sciences, of the U.S. DOE under Contract Number DEAC02-05CH11231.

## References


1. Criegee, R., Mechanism of Ozonolysis. *Angew. Chem. Int. Ed.* **1975,** *14*, 745-752.
2. Criegee, R.; Wenner, G., Die Ozonisierung des 9,10-Oktalins. *Liebigs Ann. Chem.* **1949,** *564*, 9-15.
3. Johnson, D.; Marston, G., The gas-phase ozonolysis of unsaturated volatile organic compounds in the troposphere. *Chem. Soc. Rev.* **2008,** *37*, 699-716.
4. Donahue, N. M.; Drozd, G. T.; Epstein, S. A.; Presto, A. A.; Kroll, J. H., Adventures in ozoneland: down the rabbit-hole. *Phys. Chem. Chem. Phys.* **2011,** *13*, 10848-10857.
5. Kroll, J. H.; Clarke, J. S.; Donahue, N. M.; Anderson, J. G., Mechanism of $HO_x$ Formation in the Gas-Phase Ozone−Alkene Reaction. 1. Direct, Pressure-Dependent Measurements of Prompt OH Yields. *J. Phys. Chem. A* **2001,** *105*, 1554-1560.
6. Kroll, J. H.; Sahay, S. R.; Anderson, J. G.; Demerjian, K. L.; Donahue, N. M., Mechanism of $HO_x$ Formation in the Gas-Phase Ozone-Alkene Reaction. 2. Prompt versus Thermal Dissociation of Carbonyl Oxides to Form OH. *J. Phys. Chem. A* **2001,** *105*, 4446-4457.
7. Liu, F.; Beames, J. M.; Petit, A. S.; McCoy, A. B.; Lester, M. I., Infrared-driven unimolecular reaction of $CH_3CHOO$ Criegee intermediates to OH radical products. *Science* **2014,** *345*, 1596-1598.
8. Fang, Y.; Liu, F.; Barber, V. P.; Klippenstein, S. J.; McCoy, A. B.; Lester, M. I., Communication: Real time observation of unimolecular decay of Criegee intermediates to OH radical products. *J. Chem. Phys.* **2016,** *144*, 061102.
9. Ryzhkov, A. B.; Ariya, P. A., A theoretical study of the reactions of parent and substituted Criegee intermediates with water and the water dimer. *Phys. Chem. Chem. Phys.* **2004,** *6*, 5042-5050.
10. Anglada, J. M.; González, J.; Torrent-Sucarrat, M., Effects of the substituents on the reactivity of carbonyl oxides. A theoretical study on the reaction of substituted carbonyl oxides with water. *Phys. Chem. Chem. Phys.* **2011,** *13*, 13034-13045.
11. Leather, K. E.; McGillen, M. R.; Cooke, M. C.; Utembe, S. R.; Archibald, A. T.; Jenkin, M. E.; Derwent, R. G.; Shallcross, D. E.; Percival, C. J., Acid-yield measurements of the gas-phase ozonolysis of ethene as a function of humidity using Chemical Ionisation Mass Spectrometry (CIMS). *Atmos. Chem. Phys.* **2012,** *12*, 469-479.
12. Chao, W.; Hsieh, J.-T.; Chang, C.-H.; Lin, J. J.-M., Direct kinetic measurement of the reaction of the simplest Criegee intermediate with water vapor. *Science* **2015,** *347*, 751.
13. Welz, O.; Savee, J. D.; Osborn, D. L.; Vasu, S. S.; Percival, C. J.; Shallcross, D. E.; Taatjes, C. A., Direct Kinetic Measurements of Criegee Intermediate ($CH_2OO$) Formed by Reaction of $CH_2I$ with $O_2$. *Science* **2012,** *335*, 204-207.
14. Taatjes, C. A.; Welz, O.; Eskola, A. J.; Savee, J. D.; Scheer, A. M.; Shallcross, D. E.; Rotavera, B.; Lee, E. P. F.; Dyke, J. M.; Mok, D. K. W.; Osborn, D. L.; Percival, C. J., Direct Measurements of Conformer-Dependent Reactivity of the Criegee Intermediate $CH_3CHOO$. *Science* **2013,** *340*, 177-180.
15. Sarwar, G.; Simon, H.; Fahey, K.; Mathur, R.; Goliff, W. S.; Stockwell, W. R., Impact of sulfur dioxide oxidation by Stabilized Criegee Intermediate on sulfate. *Atmos. Environ.* **2014,** *85*, 204-214.
16. Berndt, T.; Jokinen, T.; Sipilä, M.; Mauldin, R. L.; Herrmann, H.; Stratmann, F.; Junninen, H.; Kulmala, M., $H_2SO_4$ formation from the gas-phase reaction of stabilized Criegee Intermediates with $SO_2$: Influence of water vapour content and temperature. *Atmos. Environ.* **2014,** *89*, 603-612.

17. Chhantyal-Pun, R.; Davey, A.; Shallcross, D. E.; Percival, C. J.; Orr-Ewing, A. J., A kinetic study of the $CH_2OO$ Criegee intermediate self-reaction, reaction with $SO_2$ and unimolecular reaction using cavity ring-down spectroscopy. *Phys. Chem. Chem. Phys.* **2015,** *17*, 3617-3626.
18. Misiewicz, J. P.; Elliott, S. N.; Moore, K. B.; Schaefer, H. F., Re-examining ammonia addition to the Criegee intermediate: converging to chemical accuracy. *Phys. Chem. Chem. Phys.* **2018,** *20*, 7479-7491.
19. Jørgensen, S.; Gross, A., Theoretical Investigation of the Reaction between Carbonyl Oxides and Ammonia. *J. Phys. Chem. A* **2009,** *113*, 10284-10290.
20. Welz, O.; Eskola, A. J.; Sheps, L.; Rotavera, B.; Savee, J. D.; Scheer, A. M.; Osborn, D. L.; Lowe, D.; Murray Booth, A.; Xiao, P.; Anwar H. Khan, M.; Percival, C. J.; Shallcross, D. E.; Taatjes, C. A., Rate Coefficients of C1 and C2 Criegee Intermediate Reactions with Formic and Acetic Acid Near the Collision Limit: Direct Kinetics Measurements and Atmospheric Implications. *Angew. Chem. Int. Ed.* **2014,** *53*, 4547-4550.
21. Chhantyal-Pun, R.; McGillen, M. R.; Beames, J. M.; Khan, M. A. H.; Percival, C. J.; Shallcross, D. E.; Orr-Ewing, A. J., Temperature-Dependence of the Rates of Reaction of Trifluoroacetic Acid with Criegee Intermediates. *Angew. Chem. Int. Ed.* **2017,** *56*, 9044-9047.
22. Wei, W.-M.; Yang, X.; Zheng, R.-H.; Qin, Y.-D.; Wu, Y.-K.; Yang, F., Theoretical studies on the reactions of the simplest Criegee intermediate $CH_2OO$ with $CH_3CHO$. *Phys. Chem. Chem. Phys.* **2015,** *1074*, 142-149.
23. Jalan, A.; Allen, J. W.; Green, W. H., Chemically activated formation of organic acids in reactions of the Criegee intermediate with aldehydes and ketones. *Phys. Chem. Chem. Phys.* **2013,** *15*, 16841-16852.
24. Elsamra, R. M. I.; Jalan, A.; Buras, Z. J.; Middaugh, J. E.; Green, W. H., Temperature- and Pressure-Dependent Kinetics of $CH_2OO + CH_3COCH_3$ and $CH_2OO + CH_3CHO$: Direct Measurements and Theoretical Analysis. *Int. J. Chem. Kinet.* **2016,** *48*, 474-488.
25. McGillen, M. R.; Curchod, B. F. E.; Chhantyal-Pun, R.; Beames, J. M.; Watson, N.; Khan, M. A. H.; McMahon, L.; Shallcross, D. E.; Orr-Ewing, A. J., Criegee Intermediate–Alcohol Reactions, A Potential Source of Functionalized Hydroperoxides in the Atmosphere. *ACS Earth Space Chem.* **2017,** *1*, 664-672.
26. Tadayon, S. V.; Foreman, E. S.; Murray, C., Kinetics of the Reactions between the Criegee Intermediate $CH_2OO$ and Alcohols. *J.Phys. Chem. A* **2018,** *122*, 258-268.
27. Lin, Y.-H.; Yin, C.; Lin, W.-H.; Li, Y.-L.; Takahashi, K.; Lin, J. J.-M., Criegee Intermediate Reaction with Alcohol Is Enhanced by a Single Water Molecule. *J. Phys. Chem. Lett.* **2018,** *9*, 7040-7044.
28. Chao, W.; Lin, Y.-H.; Yin, C.; Lin, W.-H.; Takahashi, K.; Lin, J. J.-M., Temperature and isotope effects in the reaction of $CH_3CHOO$ with methanol. *Phys. Chem. Chem. Phys.* **2019,** *21*, 13633-13640.
29. Cabezas, C.; Endo, Y., Probing Criegee intermediate reactions with methanol by FTMW spectroscopy. *Phys. Chem. Chem. Phys.* **2020,** *22*, 13756-13763.
30. Enami, S.; Colussi, A. J., Reactions of Criegee Intermediates with Alcohols at Air–Aqueous Interfaces. *J. Phys. Chem. A* **2017,** *121*, 5175-5182.
31. Sakamoto, Y.; Yajima, R.; Inomata, S.; Hirokawa, J., Water vapour effects on secondary organic aerosol formation in isoprene ozonolysis. *Phys. Chem. Chem. Phys.* **2017,** *19*, 3165-3175.

32. Jr-Min Lin, J.; Chao, W., Structure-dependent reactivity of Criegee intermediates studied with spectroscopic methods. *Chem. Soc. Rev.* **2017,** *46*, 7483-7497.
33. Rousso, A. C.; Hansen, N.; Jasper, A. W.; Ju, Y., Identification of the Criegee intermediate reaction network in ethylene ozonolysis: impact on energy conversion strategies and atmospheric chemistry. *Phys. Chem. Chem. Phys.* **2019,** *21*, 7341-7357.
34. Sun, W.; Ju, Y., Nonequilibrium Plasma-Assisted Combustion: A Review of Recent Progress. *J. Plasma Fusion Res.* **2013,** *89*, 208-219.
35. Ju, Y.; Sun, W., Plasma assisted combustion: Dynamics and chemistry. *Prog. Energy Combust. Sci.* **2015,** *48*, 21-83.
36. Sun, W.; Gao, X.; Wu, B.; Ombrello, T., The effect of ozone addition on combustion: Kinetics and dynamics. *Prog. Energy Combust. Sci.* **2019,** *73*, 1-25.
37. Martinez, R. I.; Herron, J. T., Stopped-Flow Studies of the Mechanism of Ozone-Alkene Reactions in the Gas Phase: trans-2-butene. *J. Phys. Chem* **1988,** *92*, 4644-4648.
38. Martinez, R. I.; Herron, J. T.; Huie, R. E., The mechanism of ozone-alkene reactions in the gas phase. A mass spectrometric study of the reactions of eight linear and branched-chain alkenes. *J. Am. Chem. Soc.* **1981,** *103*, 3807-3820.
39. Atkinson, R.; Aschmann, S. M., Hydroxyl radical production from the gas-phase reactions of ozone with a series of alkenes under atmospheric conditions. *Environ. Sci. Technol.* **1993,** *27*, 1357-1363.
40. Tuazon, E. C.; Aschmann, S. M.; Arey, J.; Atkinson, R., Products of the Gas-Phase Reactions of $O_3$ with a Series of Methyl-Substituted Ethenes. *Environ. Sci. Technol.* **1997,** *31*, 3004-3009.
41. Orzechowska, G. E.; Paulson, S. E., Production of OH radicals from the reactions of C4–C6 internal alkenes and styrenes with ozone in the gas phase. *Atmos. Environ.* **2002,** *36*, 571-581.
42. Moshammer, K.; Jasper, A. W.; Popolan-Vaida, D. M.; Lucassen, A.; Diévart, P.; Selim, H.; Eskola, A. J.; Taatjes, C. A.; Leone, S. R.; Sarathy, S. M.; Ju, Y.; Dagaut, P.; Kohse-Höinghaus, K.; Hansen, N., Detection and Identification of the Keto-Hydroperoxide ($HOOCH_2OCHO$) and Other Intermediates during Low-Temperature Oxidation of Dimethyl Ether. *J. Phys. Chem. A* **2015,** *119*, 7361-7374.
43. Dagaut, P.; Cathonnet, M.; Rouan, J. P.; Foulatier, R.; Quilgars, A.; Boettner, J. C.; Gaillard, F.; James, H., A jet-stirred reactor for kinetic studies of homogeneous gas-phase reactions at pressures up to ten atmospheres (≈1 MPa). *J. Phys. E Sci Instrum.* **1986,** *19*, 207-209.
44. Azay, P.; Côme, G.-M., Temperature Gradients in a Continuous Flow Stirred Tank Reactor. *Ind. Eng. Chem. Process Des. Dev.* **1979,** *18*, 754-756.
45. Orphal, J.; Staehelin, J.; Tamminen, J.; Braathen, G.; De Backer, M.-R.; Bais, A.; Balis, D.; Barbe, A.; Bhartia, P. K.; Birk, M.; Burkholder, J. B.; Chance, K.; von Clarmann, T.; Cox, A.; Degenstein, D.; Evans, R.; Flaud, J.-M.; Flittner, D.; Godin-Beekmann, S.; Gorshelev, V.; Gratien, A.; Hare, E.; Janssen, C.; Kyrölä, E.; McElroy, T.; McPeters, R.; Pastel, M.; Petersen, M.; Petropavlovskikh, I.; Picquet-Varrault, B.; Pitts, M.; Labow, G.; Rotger-Languereau, M.; Leblanc, T.; Lerot, C.; Liu, X.; Moussay, P.; Redondas, A.; Van Roozendael, M.; Sander, S. P.; Schneider, M.; Serdyuchenko, A.; Veefkind, P.; Viallon, J.; Viatte, C.; Wagner, G.; Weber, M.; Wielgosz, R. I.; Zehner, C., Absorption cross-sections of ozone in the ultraviolet and visible spectral regions: Status report 2015. *J. Mol. Spectrosc.* **2016,** *327*, 105-121.

46. Heimann, P. A.; Koike, M.; Hsu, C. W.; Blank, D.; Yang, X. M.; Suits, A. G.; Lee, Y. T.; Evans, M.; Ng, C. Y.; Flaim, C.; Padmore, H. A., Performance of the vacuum ultraviolet high-resolution and high-flux beamline for chemical dynamics studies at the Advanced Light Source. *Rev. Sci. Instrum* **1997,** *68*, 1945-1951.
47. Leone, S. R.; Ahmed, M.; Wilson, K. R., Chemical dynamics, molecular energetics, and kinetics at the synchrotron. *Phys. Chem. Chem. Phys.* **2010,** *12*, 6564-6578.
48. Schenk, M.; Leon, L.; Moshammer, K.; Oßwald, P.; Zeuch, T.; Seidel, L.; Mauss, F.; Kohse-Höinghaus, K., Detailed Mass Spectrometric and Modeling Study of Isomeric Butene flames. *Comb. Flame* **2013,** *160*, 487-503.
49. Egolfopoulos, F. N.; Hansen, N.; Ju, Y.; Kohse-Hoinghaus, K.; Law, C. K.; Qi, F., Advances and Challenges in Laminar Flame Experiments and Implications for Combustion Chemistry. *Prog. Energy Combust. Sci.* **2014,** *43*, 36-67.
50. O' Boyle, N. M.; Banck, M.; James, C. A.; Morley, C.; Vandermeersch, T.; Hutchison, G. R., Open Babel: An open chemical toolbox. *J.Cheminformatics* **2011,** *3*, 33.
51. The Open Babel Package, V. http://openbabel.org.
52. Rousso, A. C.; Hansen, N.; Jasper, A. W.; Ju, Y., Low-temperature oxidation of ethylene by ozone in a jet-stirred reactor. *J. Phys. Chem. A* **2018,** *122*, 8674-8685.
53. Hansen, N.; Klippenstein, S. J.; Westmoreland, P. R.; Kasper, T.; Kohse-Hoinghaus, K.; Wang, J.; Cool, T. A., A combined ab initio and photoionization mass spectrometric study of polyynes in fuel-rich flames. *Phys. Chem. Chem. Phys.* **2008,** *10*, 366-374.
54. Hansen, N.; Cool, T. A.; Westmoreland, P. R.; Kohse-Höinghaus, K., Recent contributions of flame-sampling molecular-beam mass spectrometry to a fundamental understanding of combustion chemistry. *Progress in Energy and Combustion Science* **2009,** *35*, 168-191.
55. Hansen, N.; Klippenstein, S. J.; Miller, J. A.; Wang, J.; Cool, T. A.; Law, M. E.; Westmoreland, P. R.; Kasper, T.; Kohse-Höinghaus, K., Identification of $C_5H_x$ Isomers in Fuel-Rich Flames by Photoionization Mass Spectrometry and Electronic Structure Calculations. *J. Phys. Chem. A* **2006,** *110*, 4376-4388.
56. Hansen, N.; Klippenstein, S. J.; Taatjes, C. A.; Miller, J. A.; Wang, J.; Cool, T. A.; Yang, B.; Yang, R.; Wei, L.; Huang, C.; Wang, J.; Qi, F.; Law, M. E.; Westmoreland, P. R., Identification and Chemistry of $C_4H_3$ and $C_4H_5$ Isomers in Fuel-Rich Flames. *J. Phys. Chem. A* **2006,** *110*, 3670-3678.
57. Zhao, H.; Yang, X.; Ju, Y., Kinetic studies of ozone assisted low temperature oxidation of dimethyl ether in a flow reactor using molecular-beam mass spectrometry. *Comb. Flame* **2016,** *173*, 187-194.
58. Curran, H. J., Developing detailed chemical kinetic mechanisms for fuel combustion. *Proc. Comb. Inst* **2019,** *37*, 57-81.
59. Fenard, Y.; Dagaut, P.; Dayma, G.; Halter, F.; Foucher, F., Experimental and kinetic modeling study of trans-2-butene oxidation in a jet-stirred reactor and a combustion bomb. *Proc. Comb. Inst* **2015,** *35*, 317-324.
60. Li, Y.; Zhou, C.-W.; Somers, K. P.; Zhang, K.; Curran, H. J., The Oxidation of 2-Butene: A High Pressure Ignition Delay, Kinetic Modeling Study and Reactivity Comparison with Isobutene and 1-Butene. *Proc. Comb. Inst.* **2017,** *36*, 403-411.
61. Liu, F.; Fang, Y.; Kumar, M.; Thompson, W. H.; Lester, M. I., Direct observation of vinyl hydroperoxide. *Phys. Chem. Chem. Phys.* **2015,** *17*, 20490-20494.
62. Huang, C.; Yang, B.; Zhang, F., Calculation of the absolute photoionization cross-sections for C1–C4 Criegee intermediates and vinyl hydroperoxides. *J. Chem. Phys.* **2019,** *150*,

164305.
63. Porterfield, J. P.; Baraban, J. H.; Troy, T. P.; Ahmed, M.; McCarthy, M. C.; Morgan, K. M.; Daily, J. W.; Nguyen, T. L.; Stanton, J. F.; Ellison, G. B., Pyrolysis of the Simplest Carbohydrate, Glycolaldehyde (CHO−$CH_2$OH), and Glyoxal in a Heated Microreactor. *J. Phys. Chem. A* **2016,** *120*, 2161-2172.
64. Leach, S.; Schwell, M.; Jochims, H.-W.; Baumgärtel, H., VUV photophysics of acetic acid: Fragmentation, fluorescence and ionization in the 6–23eV region. *Chem. Phys.* **2006,** *321*, 171-182.
65. Wang, J.; Yang, B.; Cool, T. A.; Hansen, N., Absolute cross-sections for dissociative photoionization of some small esters. *Int. J. Mass Spectrom.* **2010,** *292*, 14-22.
66. Martinez, R. I., Alkenoxy radicals in gas-phase reactions of alkenes with oxygen atoms or ozone. *Chem. Phys. Let.* **1983,** *98*, 507-510.
67. Story, P. R.; Burgess, J. R., Ozonolysis. Evidence for carbonyl oxide tautomerization and for 1,3-dipolar addition to olefins. *J. Am. Chem. Soc.* **1967,** *89*, 5726-5727.
68. Vereecken, L.; Harder, H.; Novelli, A., The reactions of Criegee intermediates with alkenes, ozone, and carbonyl oxides. *Phys. Chem. Chem. Phys.* **2014,** *16*, 4039-4049.
69. Pfeifle, M.; Ma, Y.-T.; Jasper, A. W.; Harding, L. B.; Hase, W. L.; Klippenstein, S. J., Nascent energy distribution of the Criegee intermediate $CH_2OO$ from direct dynamics calculations of primary ozonide dissociation. *J. Chem. Phys.* **2018,** *148*, 174306.
70. Rodriguez, A.; Herbinet, O.; Wang, Z.; Qi, F.; Fittschen, C.; Westmoreland, P. R.; Battin-Leclerc, F., Measuring hydroperoxide chain-branching agents during n-pentane low-temperature oxidation. *Proc. Comb. Inst.* **2017,** *36*, 333-342.
71. Rodriguez, A.; Herbinet, O.; Meng, X.; Fittschen, C.; Wang, Z.; Xing, L.; Zhang, L.; Battin-Leclerc, F., Hydroperoxide Measurements During Low-Temperature Gas-Phase Oxidation of n-Heptane and n-Decane. *J. Phys. Chem. A* **2017,** *121*, 1861-1876.
72. Atkinson, R., Gas-Phase Tropospheric Chemistry of Volatile Organic Compounds: 1. Alkanes and Alkenes. *J. Phys. Chem. Ref. Data* **1997,** *26*, 215-290.
73. Jenkin, M. E.; Saunders, S. M.; Pilling, M. J., The tropospheric degradation of volatile organic compounds: a protocol for mechanism development. *Atmos. Environ.* **1997,** *31*, 81-104.
74. Jackson, A.; Hewitt, C., Atmosphere Hydrogen Peroxide and Organic Hydroperoxides: A Review. *Crit. Rev. Environ. Sci. Technol.* **1999,** *29*, 175-228.
75. Lee, M.; Heikes, B. G.; O'Sullivan, D. W., Hydrogen peroxide and organic hydroperoxide in the troposphere: a review. *Atmos. Environ.* **2000,** *34*, 3475-3494.
76. Yin, C.; Takahashi, K., How does substitution affect the unimolecular reaction rates of Criegee intermediates? *Phys. Chem. Chem. Phys.* **2017,** *19*, 12075-12084.
77. Anglada, J. M.; Aplincourt, P.; Bofill, J. M.; Cremer, D., Atmospheric formation of OH radicals and $H_2O_2$ from alkene ozonolysis under humid conditions. *ChemPhysChem* **2002,** *3*, 215-221.
78. Sheps, L.; Scully, A. M.; Au, K., UV absorption probing of the conformer-dependent reactivity of a Criegee intermediate $CH_3CHOO$. *Phys. Chem. Chem. Phys.* **2014,** *16*, 26701-26706.
79. Cabezas, C.; Endo, Y., The reactivity of the Criegee intermediate $CH_3CHOO$ with water probed by FTMW spectroscopy. *J. Chem. Phys.* **2018,** *148*, 014308.
80. Lin, L.-C.; Chao, W.; Chang, C.-H.; Takahashi, K.; Lin, J. J.-M., Temperature dependence of the reaction of anti-$CH_3CHOO$ with water vapor. *Phys. Chem. Chem. Phys.* **2016,** *18*,

28189-28197.
81. Cabezas, C.; Endo, Y., Observation of hydroperoxyethyl formate from the reaction between the methyl Criegee intermediate and formic acid. *Phys. Chem. Chem. Phys.* **2020,** *22*, 446-454.
82. Heikes, B. G.; Chang, W.; Pilson, M. E. Q.; Swift, E.; Singh, H. B.; Guenther, A.; Jacob, D. J.; Field, B. D.; Fall, R.; Riemer, D.; Brand, L., Atmospheric methanol budget and ocean implication. *Glob. Biogeochem. Cycles* **2002,** *16*, 80-1-80-13.
83. Mellouki, A.; Wallington, T. J.; Chen, J., Atmospheric Chemistry of Oxygenated Volatile Organic Compounds: Impacts on Air Quality and Climate. *Chem. Rev.* **2015,** *115*, 3984-4014.
84. Stavrakou, T.; Guenther, A.; Razavi, A.; Clarisse, L.; Clerbaux, C.; Coheur, P. F.; Hurtmans, D.; Karagulian, F.; De Mazière, M.; Vigouroux, C.; Amelynck, C.; Schoon, N.; Laffineur, Q.; Heinesch, B.; Aubinet, M.; Rinsland, C.; Müller, J. F., First space-based derivation of the global atmospheric methanol emission fluxes. *Atmos. Chem. Phys.* **2011,** *11*, 4873-4898.